A Numerical Investigation into Size Effects in Centre-Notched Quasi-isotropic Carbon/Epoxy Laminates

Xiaodong Xu[a]*, Michael R. Wisnom[a], Xiangqian Li[a], Stephen R. Hallett[a]

[a] Advanced Composites Centre for Innovation & Science (ACCIS), University of Bristol, University Walk, Bristol BS8 1TR, UK

ABSTRACT

Numerical modelling of scaled centre-notched $[45/90/-45/0]_{4s}$ carbon/epoxy laminates was carried out. The in-plane dimensions of the models were scaled up by a factor of up to 16. A Finite Element (FE) method using the explicit code LS-Dyna was applied to study the progressive damage development at the notch tips. Cohesive interface elements were used to simulate splits within plies and delaminations between plies. A failure criterion based on Weibull statistics was used to account for fibre failure. There is a good correlation between the numerical and experimental results, and the scaling trend can be explained in terms of the growth of the notch tip damage zone. The modelling gives new insights into the damage development in the quasi-isotropic laminates with sharp cracks, specifically, the growth of splits, delaminations and local fibre breakage.

Keywords: A. Laminate; B. Strength; C. Finite element analysis (FEA); C. Notch; Size effect

* Corresponding author. Tel.: +44 (0)117 33 15775.
E-mail address: xiaodong.xu@bristol.ac.uk (X. Xu)

1. Introduction

Notched tensile strength of composites is a critical design driver. For example, notched tensile tests are important to determine the damage tolerance of composite fuselage structures. The sizes of laboratory notched coupons are usually at the scale of centimetres. In contrast, large composite structures are normally sized in metres. There is an obvious dimension gap, so it is important to understand the relationship between the notched tensile strength of the small coupons and that of the large structures.

A few numerical methods were used to investigate the size effects in notched composite laminates [1-4]. These approaches did not simulate the detailed damage development at the notches. As a result, they need additional fracture parameters (e.g. trans-laminar fracture toughness) in order to capture the scaling of strength. In contrast, this paper adopts a virtual test technique which simulates the detailed notch-tip damage development at different load levels and in different specimen sizes.

Discrete transverse crack and delamination were found to be crucial mechanisms in the failure of composite laminates [5]. For example, splitting and delamination can significantly affect the stress gradient at the notch tip. Different numerical approaches have been developed to study fracture and damage in composites, such as continuum modelling [6-8], embedded crack modelling, e.g. eXtended Finite Element Method (X-FEM) [9] and discrete modelling, e.g. cohesive interface methods [5, 10, 11]. Among the above modelling techniques, numerical methods have been developed to simulate matrix cracking and delamination initiating from free edges [12-14], and those initiating from notches [9, 15, 16]. Compared with continuum damage modelling, cohesive interface methods can better represent the physical mechanisms at the discontinuities that arise at the discrete failures. There may be scope to apply the X-FEM approach in

the future, but that would require further development to combine with the Weibull statistics based criterion for fibre breakage which is crucial in the current study.

A numerical technique using the explicit FE code LS-Dyna and cohesive interface elements was developed to simulate the sub-critical damage in composite laminates with open holes [17] and sharp cracks [18]. Such detailed modelling technique can successfully predict the tensile strength of open-hole specimens and blocked-ply over-height compact tension specimens. In those cases, the final failure follows immediately from the first fibre failure. However, the dispersed-ply laminates with sharp cracks were not well simulated, in which the first fibre failure does not lead to the final failure straight away. Instead, a damage zone which consists of stable fibre breakage, multiple splits and delaminations is observed at the crack tips [19]. Simulating the first fibre failure alone is not enough, and simulation of the development of the damage zone and its influence on progressive fibre failure is necessary for accurate predictions.

An experimental investigation into the size effects in in-plane scaled centre-notched $[45/90/-45/0]_{4s}$ laminates has recently been conducted [19]. The damage zone was shown to play an important role in the scaling of centre-notched tensile strength. The centre-notched strength decreases towards a Linear Elastic Fracture Mechanics (LEFM) asymptote as the notch length increases, with the size of the damage zone approaching an approximately constant value. In the present paper, the damage development in in-plane scaled centre-notched $[45/90/-45/0]_{4s}$ laminates was studied through an FE approach based on that of Li et al. [18]. The sizes of the simulated damage zones in the scaled models were compared with those in the CT images from interrupted tests [19], which has not hitherto been done. Because the scaled FE models simulate closely the damage zone behaviour, the size effects can be well represented

and explained in terms of the growth of the damage zone, which can be observed in much greater detail than is usually possible experimentally. Using this information to provide understanding of the mechanisms giving rise to the size effects in sharp notched specimens is the main novelty of this paper.

2. Experimental specimen configuration modelled

A schematic of the in-plane scaled centre-notched specimens and their dimensions are illustrated in Fig. 1. Detailed ply-by-ply 3D FE models with 8-node constant stress solid elements are constructed in LS-Dyna. All nodes at its one end are fixed, with uniform displacements applied to the nodes at the other end. Half thickness of each specimen is modelled, with symmetric boundary conditions applied to the nodes at the mid-plane. The in-plane dimensions of the quasi-isotropic specimens were scaled up by a factor of up to 8. In addition, a larger specimen with only the width and notch length doubled from the one-size-smaller specimens (named as the "short variant") was also modelled as a further comparison. FE analysis demonstrated that in the short variant specimens the closer boundaries in the length direction do not affect the stress distribution near the notches.

The material used in the tests was Hexcel HexPly® IM7/8552 carbon-epoxy pre-preg with a nominal ply thickness of 0.125 mm. All specimens were of the same $[45/90/-45/0]_{4s}$ layup. The nominal thickness was 4 mm, which is very close to the actual specimen thickness of 4 mm (C.V. 1.4%).

3. FE model setup

3.1. Typical FE mesh

Fig. 2 illustrates a typical FE mesh. A triangular shaped sharp notch tip was modelled. In the experiments, a 0.25 mm-wide notch tip was cut with a piercing saw

blade, which was proved to be sharp enough not to affect the measured fracture toughness in Ref. [19]. The CT images from the experimental study show that fibre breakage is usually constrained within ±45° lines starting from the notch tips. So in the FE analysis, a refined mesh was arranged near the notch tips within the ±45° lines to be able to simulate the progressive damage development. A coarser mesh was used outside this region.

The models were set up with a nominal ply thickness of 0.125 mm, so have a thickness of 4 mm, similar to the measured value of 4 mm (C.V. 1.4%). The model of the baseline specimens with one element through the thickness of each ply was compared with a model with two elements through the thickness of each ply. The results were within 1.2%, so only one element through each ply thickness was used in all of the subsequent FE models.

3.2. Cohesive interface elements

In the FE analysis, cohesive interface elements were used to simulate the splits within plies and the delaminations between plies. Specifically, to simulate the damage zone at the notch tips, multiple potential split paths in the 0° plies were pre-defined. For example, there are 9 pre-defined potential 0° split paths (marked in red) in the typical FE mesh in Fig. 2 (a). In contrast, there is only a single pre-defined potential split path, starting from each notch tip, in the plies with other orientations (±45° and 90°). This is because the models showed that there is no fibre breakage in the other plies before final failure, and no further potential split paths are needed to blunt the stress concentrations after initial fibre fracture. Additional potential split paths could have been included in these plies. However they would not affect the results and would increase computation time. Fig. 2 (b) illustrates how the potential split paths are arranged. The properties of

the cohesive interface elements are shown in Table 1 [17].The mixed-mode traction displacement relationship for cohesive interface elements is shown in Fig. 3 [20].

3.3. Fibre failure criterion

A criterion based on Weibull statistics has been used to predict fibre failure. The theory supposes that the strength of a brittle-like material is controlled by defects which follow a Weibull distribution, and the strength is related to the stressed volume [21]. When the volume adjusted stress reaches the unnotched unidirectional strength, fibre failure will occur. Using the assumption of equal probability of survival between the model and unit volume of material, we have Equation 1 [18]:

$$\int_V \left(\frac{\sigma}{\sigma_{\text{unit}}}\right)^m dV = \sum_{i=1}^{\text{Total No. of Solid Elements}} \left(\frac{\sigma_i}{\sigma_{\text{unit}}}\right)^m V_i = 1 \quad (1)$$

where, σ_i is the elemental stress, V_i is the elemental volume, $\sigma_{\text{unit}} = 3131$ MPa is the tensile strength of a unit volume of material, $m = 41$ is the Weibull modulus from scaled unnotched unidirectional tensile tests of the same material [22]. Other lamina properties are shown in Table 1 [17].

Equation 1 is checked at each time step. When this fibre failure criterion is satisfied, the element with the maximum fibre direction stress loses its load carrying capability and its contribution is removed. After this, the load is automatically redistributed to the other remaining elements. With increasing applied load, the stresses in the remaining elements keep increasing until Equation 1 is satisfied again, then the next element with the maximum fibre direction stress is degraded. This represents the continuous fibre breakage process within the damage zone [18]. The same modelling technique was successfully used to study progressive damage in over-height compact tension models [18]. It was found that once the local fibre breakage in the 0° plies initiates, it does not

propagate unstably. This is because although the first fibre breakage occurs due to the high Stress Concentration Factor (SCF) at the notch tip, there is not enough energy for it to propagate. Instead, it is arrested and secondary splits start to grow ahead of it. In the current FE analysis, Equation 1 is insufficient on its own, and needs to work together with multiple potential 0° split paths in order to simulate such damage zone behaviour.

4. FE analysis

4.1. Typical damage development

In the model of the baseline specimens (C = 3.2 mm) with 0.1 mm minimum mesh size, 9 potential split paths were pre-defined within a 1 mm distance from the notch tips in order to investigate the damage development at different load levels. The degraded elements representing fibre breakage are marked in black. The fully failed cohesive interface elements in which the critical strain energy release rate has been exceeded are marked in red, corresponding to splits and delaminations. As shown in Fig. 4, the damage develops in the following sequence: At the beginning, initial splits grow with applied stress in all the plies. Delamination then starts to occur at a higher stress level and splits with different orientations can join up. As the applied stress increases, fibre failure occurs in some 0° plies, at which point further delaminations also occur. Because the simulation is under displacement control, there is no external work done when fibres break. As the stored elastic energy is released, there is a load drop and the newly formed crack arrests. When the applied stress increases again, secondary 0° splits grow at the new crack front. The average distance between the last newly formed splits and the notch tip is measured as the size of the damage zone. After a certain amount of damage development, the fibre breakage propagates unstably across the model width, which terminates the simulation. This corresponds to the final failure in the tests and the

final load drops on the load-displacement curves in Fig. 5 (d) and Fig. 6 (c). Because of the unstable nature of the specimens, the damage status beyond 95% of failure load is extremely hard to capture experimentally. However, the modelling is able to show the stable damage development prior to catastrophic fracture which is key to understanding size effects.

4.2. Mesh dependency

The above mesh for the baseline specimens (0.1 mm) is doubled to form the Scale 2 mesh (0.2 mm). Different densities of the potential 0° split paths in the Scale 2 model are compared in Fig. 5. The FE results are illustrated in Fig. 5 (d), and were found not to be sensitive to the density of potential split paths for a spacing of 1 mm or less. The Scale 2 mesh was refined at the notch tips to form the fine mesh (0.1 mm) as shown in Fig. 6. The results in Fig. 6 (c) show a reduction only of 3.2% for the refined mesh. So the Scale 2 mesh (0.2 mm) is considered to be sufficiently refined. The results are not sensitive to the mesh sizes, because the predicted splits blunt the stress concentration at the notch tip. Although the model of the baseline specimen used a smaller 0° split spacing (0.125 mm split spacing), in order to better capture the critical size of the damage zone, the Scale 2 mesh (0.2 mm) with 1 mm split spacing was chosen as the standard mesh and was used for the scaled up models. The Scale 4, Scale 8 and Scale 16 models have approximately the same minimum absolute mesh size (0.2 mm), and a split spacing of 1 mm covering a distance of 4 mm from the crack tip. In the Scale 8 and Scale 16 models, the mesh at the crack tip is refined over a larger area in order to capture the slightly larger damage zone found subsequently in the analysis.

In other more general cases, the pre-defined multiple potential 0° split paths should cover a distance that is larger than the size of the fully developed damage zone in

the specimen. If in the analysis damage grows beyond this distance, then it needs to be extended. Initially, it is better to extend that distance across the whole width of the specimen with 1 mm or less spacing, which could later be reduced once the damage zone size is determined from the model.

4.3. Scaling of damage zones

In Fig. 7, the damage zones in the scaled FE models are compared with those in the CT images from interrupted tests, each at the same load, which is 95% of the mean experimental failure loads for each different specimen size. The FE models with pre-defined multiple potential 0° split paths can simulate the stable fibre failure propagation within the damage zone, the delamination shapes, split lengths and the trend for the increase in damage zone as a function of notch size. The size effects, i.e. the scaling of tensile strengths should therefore be able to be predicted. It can also be seen in Fig. 7 that the damage zones observed from both the interrupted tests and the FE models are approaching an asymptote.

In Fig. 8, the sub-critical damage and fibre breakage in the scaled FE models are compared at both approximately constant applied stress (340 MPa) and approximately constant strain energy release rate G (30 kJ/m^2, well below the value corresponding to fracture energy due to fibre failure) for different specimen sizes. G is calculated according to Equation 2 [23], which is valid for quasi-isotropic laminates ignoring ply level effects such as free edge stresses and damage. Equation 2 cannot be directly applied to anisotropic laminates. Although Laffan et al.[24] applied a similar equation for orthotropic laminates, they did not recommend applying it to highly orthotropic laminates.

$$G = \frac{\pi C f^2(\lambda)\sigma_g^2}{2E} \quad (2)$$

where, G is the strain energy release rate, σ_g is the applied gross section stress, $f(\lambda) = \sqrt{\sec(\pi\lambda)} = 1.025$ is a geometric parameter to account for the effect of finite width [25], C is the initial full notch length, W is specimen width, $\lambda = C/2W = 0.1$ and E = 61.6 GPa is the in-plane Young's modulus.

The stress and G values are not exactly constant due to finite output time steps used in the explicit analysis resulting in discrete values. The extent of damage is approximately the same at constant G, but increases with size at constant applied stress, which indicates that the development of the damage zone is driven by energy.

4.4. Propagation of initial 0° splits

With the available FE data, the development of damage in the scaled models was also examined in terms of the growth of the initial 0° splits at the notch tips. The FE analysis in this section is based on a simpler model, which only includes the initial potential split paths, and no fibre failure criterion. The minimum mesh size is kept the same (0.2 mm) for the scaled models.

In Fig. 9, the initial 0° split lengths increase linearly with increasing G, which implies that the initial 0° splits are driven by energy. Splits are longer in the central double 0° plies than those in the outboard single 0° plies.

The SCFs in the 0° plies in the simpler model of the baseline specimens were studied in Fig. 10 (a). The SCF is calculated by using the maximum elemental stress divided by the applied gross section stress. The SCFs decrease linearly with increasing applied stress. Fig. 10 (a) also illustrates that the central double 0° ply has a lower SCF at the same applied stress, which explains why the fibres in the central double 0° plies

break at a higher applied stress level. The reason for the lower SCF in the central double 0° ply is that the splits are longer than those in the single 0° plies at the same stress level as shown in Fig. 9, due to more energy being available in the thicker ply block.

The 0° split length at the notch tip in the scaled models is normalised by the notch length in Fig. 10 (b), and the SCFs also decrease with increasing normalised split length. This explains why the SCFs decrease with increasing applied stress, because the initial 0° splits grow with applied stress (or G) as shown in Fig. 9, which can further blunt the stress concentration at the notch tip. Fig. 10 (b) also illustrates that the central double 0° ply has a slightly lower SCF even at the same split length, because it is affected by the split lengths in the other plies.

4.5. Result comparison

There is a good correlation between the numerical and the experimental results as shown in Fig. 11. The FE result for the baseline specimens (583 MPa) is spot on, the Scale 2 specimens (542 MPa) 4.4% high, the Scale 4 specimens (489 MPa) 7.2% high, the Scale 8 specimens (412 MPa) 18.1% high and the Scale 16 specimens (291 MPa) 11.5% high, with an average difference of 8.3% for the whole set.

In Fig. 11, the LEFM scaling line is determined from the constant G_{Scale16} = 115.2 kJ/m^2 calculated from Equation 2 by using the predicted tensile strength $\sigma_{\text{g,Scale16}}$ = 291 MPa of the largest Scale 16 model. The results for the smaller specimens are below this line, but as the notch lengths increase, the tensile strengths from the larger models clearly approach the LEFM scaling line. This is consistent with the experimental study [19], and agrees with the scaling trend of the predicted damage zones which approach an approximately constant size as the simulated specimens get larger. Unfortunately it is

not computationally practical to run even larger models, and this would be of limited value since there are no experimental results to compare with.

5. Discussion

The Scaled 8 and Scale 16 models have approximately the same minimum mesh size (0.2 mm) at the notch tips to that in the Scale 2 model. However, the mesh away from the notch tips is coarser than that in the smaller models in order to make the models computationally efficient. As a result, the unstable fracture beyond the damage zone is sometimes artificially delayed when it propagates into the coarse mesh in the larger models, which contributes to the larger discrepancy between the numerical and experimental results.

The propagation of the initial 0° splits is driven by energy, as demonstrated by Fig. 9. Similarly, the development of the damage zone as a whole is driven by energy, as seen in Fig. 8. The strength of the brittle fibres follows a Weibull statistics based limit. The growth of initial splits can delay fibre failure by reducing the SCFs as shown in Fig. 10 (b) (stress blunting). Stable fibre breakage in the 0° plies can release the strain energy at the notch tips and form a damage zone, followed by arrest of the initial crack propagation and initiation of secondary splits. The failure criterion for the sub-critical damage and that for the fibres interact with each other, resulting in the observed size effects in the notched laminates. Specifically, for the smaller models, although their strengths are higher, the energy levels at final failure are actually lower. For example, according to Equation 2, the model of the baseline specimens predicts failure at $\sigma_{g,Baseline}$ = 583 MPa, so at $G_{Baseline}$ = 29.1 kJ/m^2. In contrast, the Scale 16 model predicts failure at $\sigma_{g,Scale16}$ = 291 MPa, so at $G_{Scale16}$ = 115.2 kJ/m^2. For the smaller models, the damage zones are under-developed due to lower G, and the energetic and statistical scaling laws

both contribute to the size effects, which results in an intermediate scaling trend. For the larger models, the damage zones are fully developed due to higher G, so the energetic size effect dominates, with the strength scaling approaching an LEFM scaling line and the damage zone approaching an approximately constant size.

6. Conclusions

The present detailed modelling using cohesive interface elements provides a powerful numerical tool for understanding the progressive damage development at the notch tips of the centre-notched quasi-isotropic laminates. It can simulate the interaction among different failure mechanisms within the damage zone such as splitting, delamination and fibre breakage. The FE results are not dependent on the mesh or split density provided these are fine enough and the pre-defined potential 0° split paths extend over a distance larger than the fully developed damage zone.

The development of the damage zone is studied through the detailed modelling. The present scaled FE models do not show catastrophic failure when the fibre breakage initiates. Instead, complete failure only occurs after a period of progressive fibre breakage in the 0° plies within the damage zone, which agrees with the experimental observations.

There is a good correlation between the numerical and experimental results. This is because the detailed FE modelling can represent the delamination shapes, split lengths and the scaling of the damage zone as a function of notch size. With the pre-defined multiple potential 0° split paths at the notched tips and the Weibull criterion for fibre failure, the stable fibre failure propagation within the damage zone can also be simulated. As the notch lengths increase, the tensile strengths are predicted to decrease towards an LEFM scaling line, which is consistent with the experimental study.

References

[1] Cairns DS, Ilcewicz LB, Walker T, Minguet PJ. Fracture scaling parameters of inhomogeneous microstructure in composite structures. Composites Science and Technology. 1995;53(2):223-231.

[2] Gonzáles L, Knauss WG. Scaling global fracture behavior of structures-sized laminated composites. International Journal of Fracture. 2002;118(4):363-394.

[3] Rudraraju SS, Salvi A, Garikipati K, Waas AM. In-plane fracture of laminated fiber reinforced composites with varying fracture resistance: Experimental observations and numerical crack propagation simulations. International Journal of Solids and Structures. 2010;47(7-8):901-911.

[4] Camanho PP, Erçin GH, Catalanotti G, Mahdi S, Linde P. A finite fracture mechanics model for the prediction of the open-hole strength of composite laminates. Composites Part A: Applied Science and Manufacturing. 2012;43(8):1219-1225.

[5] Wisnom MR. Modelling discrete failures in composites with interface elements. Composites Part A: Applied Science and Manufacturing. 2010;41(7):795-805.

[6] Chang FK, Chang KY. A progressive damage model for laminated composites containing stress concentrations. Journal of Composite Materials. 1987;21(9):834-855.

[7] Davila CG, Camanho PP, Rose CA. Failure criteria for FRP laminates. Journal of Composite Materials. 2005;39(4):323-345.

[8] Forghani A, Zobeiry N, Vaziri R, Poursartip A, Ellyin F. A non-local approach to simulation of damage in laminated composites. Damage in Composites. 2013;5:279-294.

[9] Mollenhauer D, Iarve EV, Kim R, Langley B. Examination of ply cracking in composite laminates with open holes: A moiré interferometric and numerical study. Composites Part A: Applied Science and Manufacturing. 2006;37(2):282-294.

[10] Pinho ST, Iannucci L, Robinson P. Formulation and implementation of decohesion elements in an explicit finite element code. Composites Part A: Applied Science and Manufacturing. 2006;37(5):778-789.

[11] Turon A, Camanho PP, Costa J, Renart J. Accurate simulation of delamination growth under mixed-mode loading using cohesive elements: Definition of interlaminar strengths and elastic stiffness. Composite Structures. 2010;92(8):1857-1864.

[12] Rybicki EF, Schmueser DW, Fox J. An energy release rate approach for stable crack growth in free-edge delamination problem. Journal of Composite Materials. 1977;11:470-487.

[13] O'Brien TK, Hooper SJ. Local delamination in laminates with angle ply matrix cracks, Part I: tension tests and stress analysis. Composite Materials: Fatigue and Fracture, ASTM STP 1156. 1993;4:491-506.

[14] Soutis C, Kashtalyan M. Delamination growth and residual properties of cracked orthotropic laminates under tensile loading. Journal of Thermoplastic Composite Materials. 2002;15(1):13-22.

[15] Kortschot MT, Beaumont PWR. Damage mechanics of composite materials: II-A damaged-based notched strength model. Composites Science and Technology. 1990;39(4):303-326.

[16] Wisnom MR, Hallett SR. The role of delamination in strength, failure mechanism and hole size effect in open hole tensile tests on quasi-isotropic laminates. Composites Part A: Applied Science and Manufacturing. 2009;40(4):335-342.

[17] Hallett SR, Green BG, Jiang WG, Wisnom MR. An experimental and numerical investigation into the damage mechanisms in notched composites. Composites Part A: Applied Science and Manufacturing. 2009;40(5):613-624.

[18] Li X, Hallett SR, Wisnom MR. Numerical investigation of progressive damage and the effect of layup in overheight compact tension tests. Composites Part A: Applied Science and Manufacturing. 2012;43(11):2137-2150.

[19] Xu X, Wisnom MR, Mahadik Y, Hallett SR. An experimental investigation into size effects in quasi-isotropic carbon/epoxy laminates with sharp and blunt notches. Composites Science and Technology. 2014;100(0):220-227.

[20] Jiang W-G, Hallett SR, Green BG, Wisnom MR. A concise interface constitutive law for analysis of delamination and splitting in composite materials and its application to scaled notched tensile specimens. International Journal for Numerical Methods in Engineering. 2007;69(9):1982-1995.

[21] Wisnom MR. Size effects in the testing of fibre-composite materials. Composites Science and Technology. 1999;59(13):1937-1957.

[22] Wisnom MR, Khan B, Hallett SR. Size effects in unnotched tensile strength of unidirectional and quasi-isotropic carbon/epoxy composites. Composite Structures. 2008;84(1):21-28.

[23] Edwalds HL, Wanhill RJH. Fracture mechanics: Edward Arnold, Delftse Uitgevers Maatschappij 1984.

[24] Laffan MJ, Pinho ST, Robinson P, Iannucci L. Measurement of the in situ ply fracture toughness associated with mode I fibre tensile failure in FRP. Part I: Data reduction. Composites Science and Technology. 2010;70(4):606-613.

[25] Newman JC. Fracture analysis of various cracked configurations in sheet and plate materials. Properties Related to Fracture Toughness ASTM STP 605. 1976:104-123.

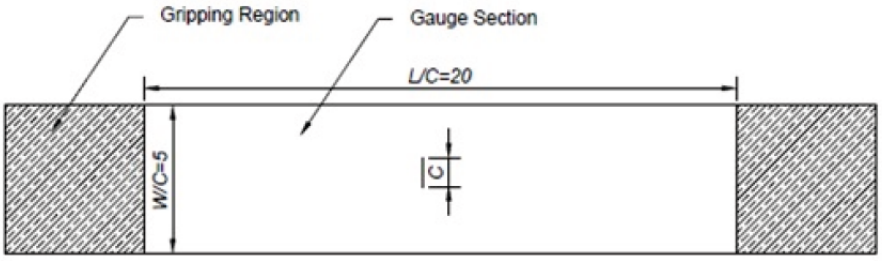

Specimens	Notch length C	Gauge width W	Gauge length L
Baseline	3.2	15.9	63.5
Scale 2	6.4	31.8	127.0
Scale 4	12.7	63.5	254.0
Scale 8	25.4	127.0	508.0
Scale 16	50.8	254.0	508.0

Fig. 1. Schematic of the in-plane scaled centre-notched specimens and dimensions (mm).

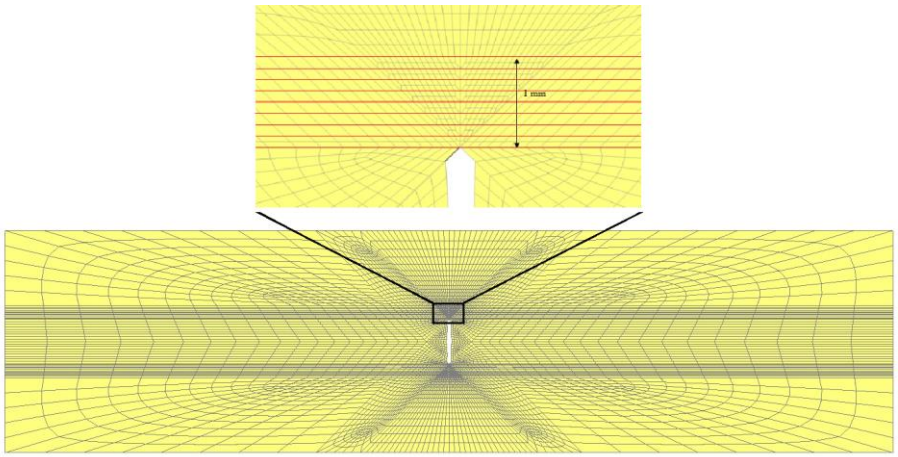

(a) Typical mesh at crack tip

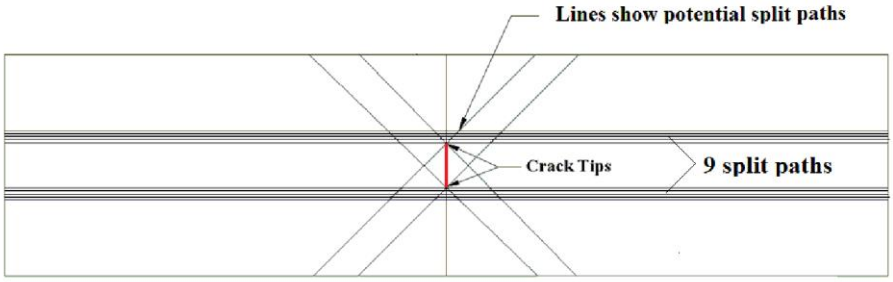

(b) Typical arrangement of potential split paths

Fig. 2. Typical FE mesh.

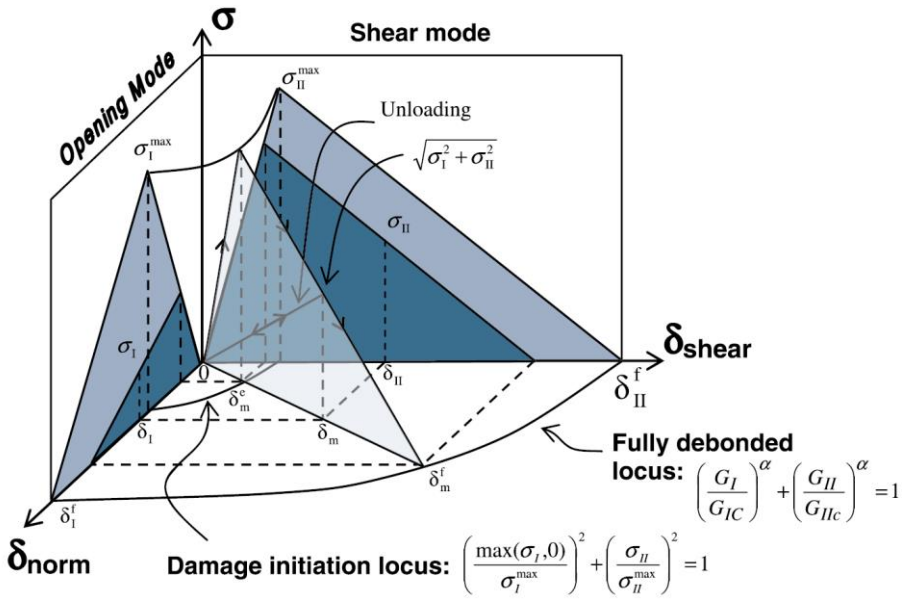

Fig. 3. Mixed-mode traction displacement relationship for cohesive interface elements.

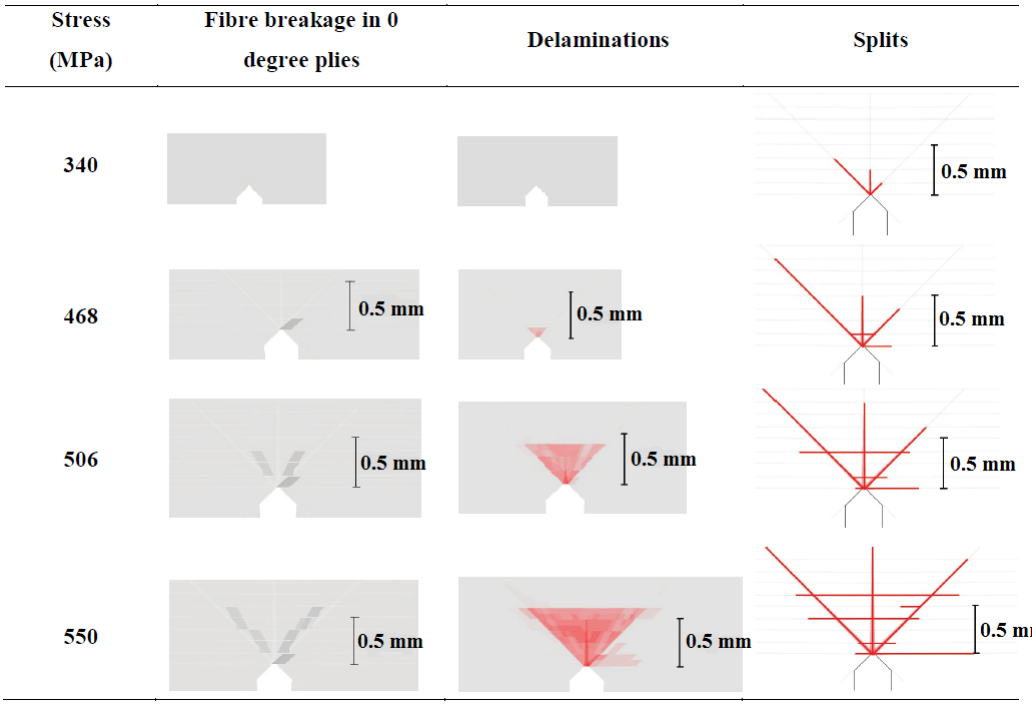

Fig. 4. Damage development in the model of baseline specimens (All layers superimposed).

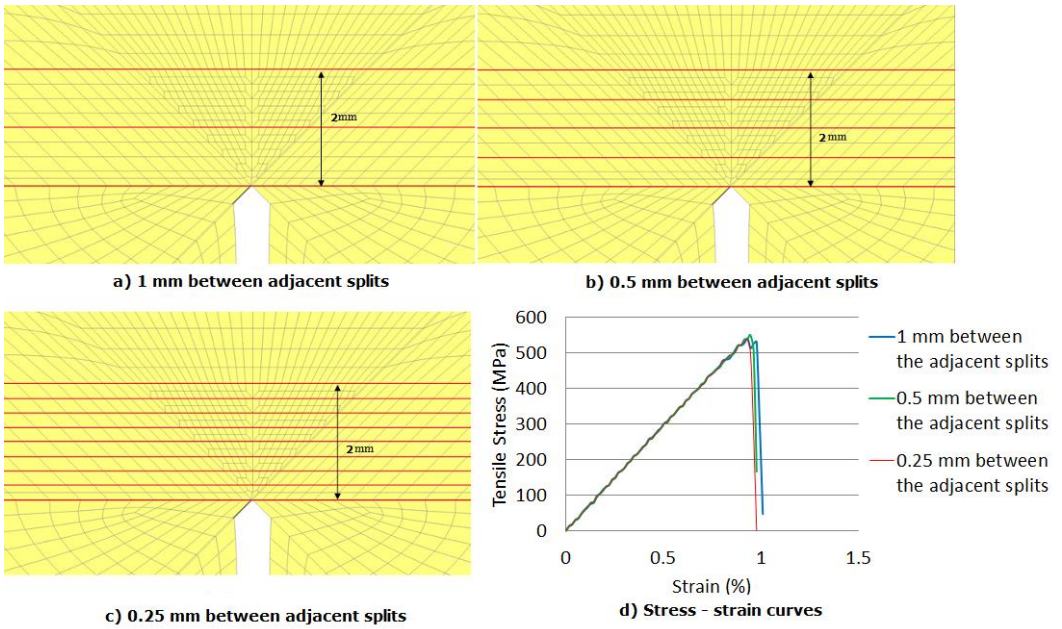

Fig. 5. Split density effects in the 0° plies in the Scale 2 model.

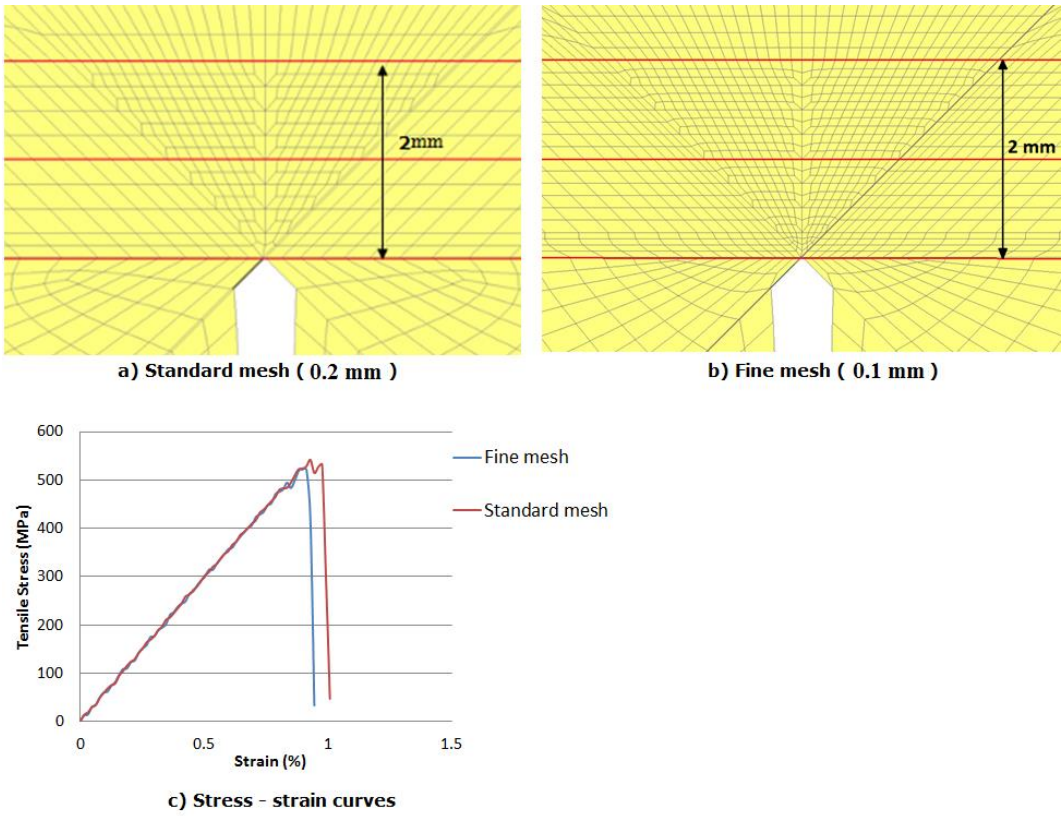

Fig. 6. Mesh size effects in the Scale 2 model.

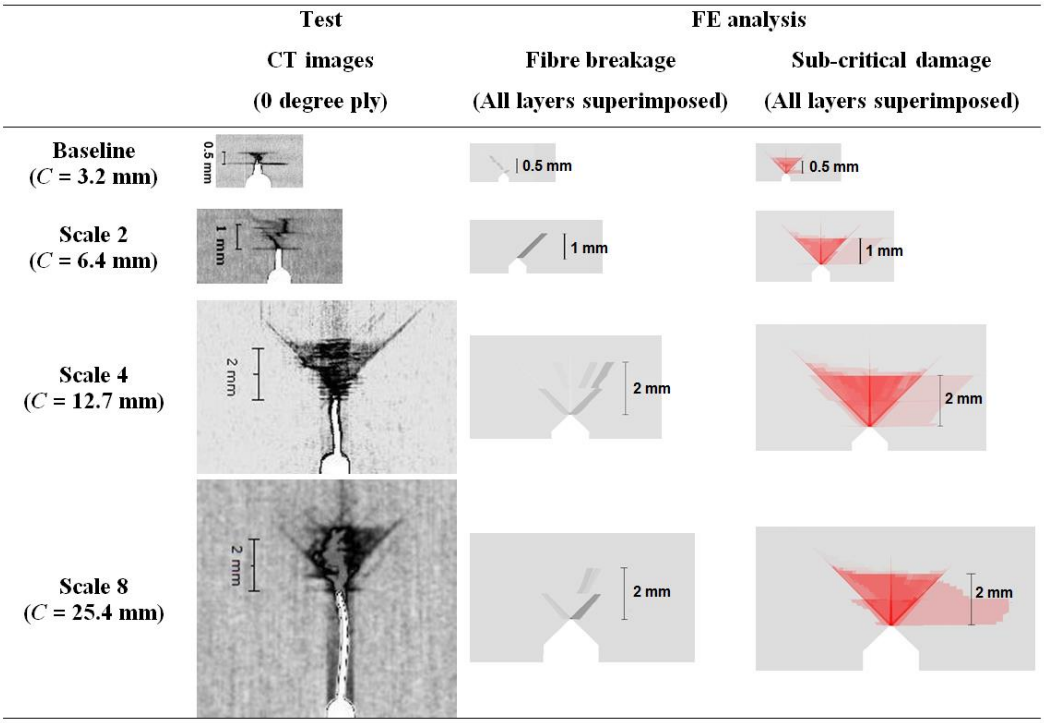

Fig. 7. Damage zone comparison at 95% of the mean experimental failure load.

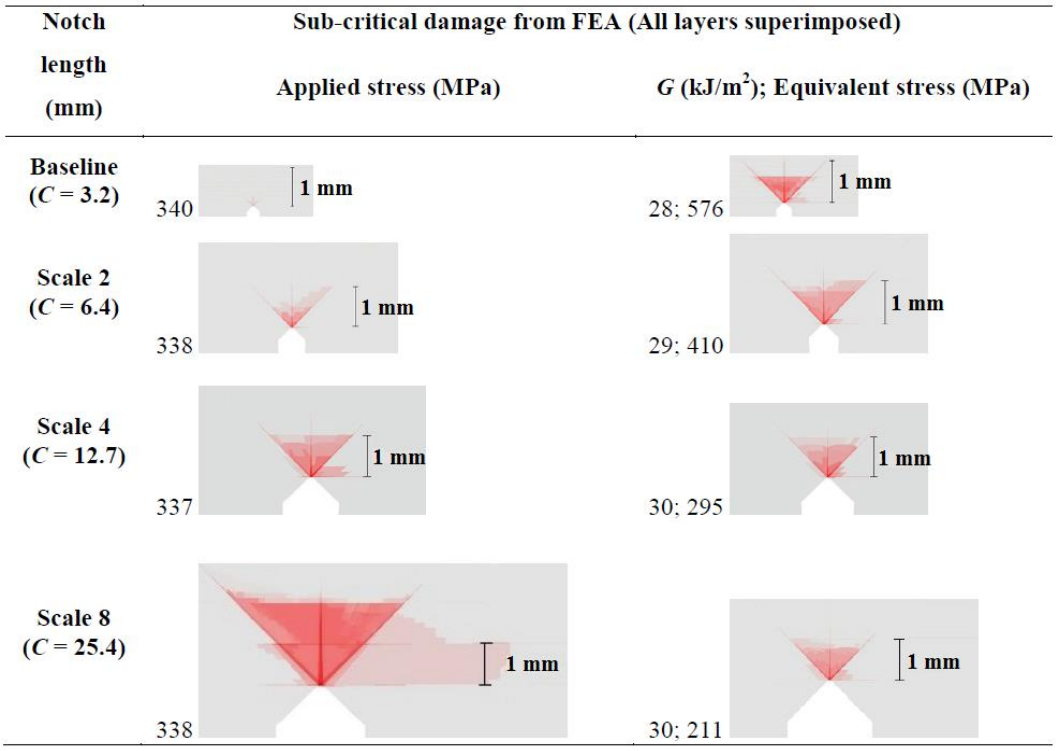

Fig. 8. Damage zone comparison at approximately constant applied stress and approximately constant *G*.

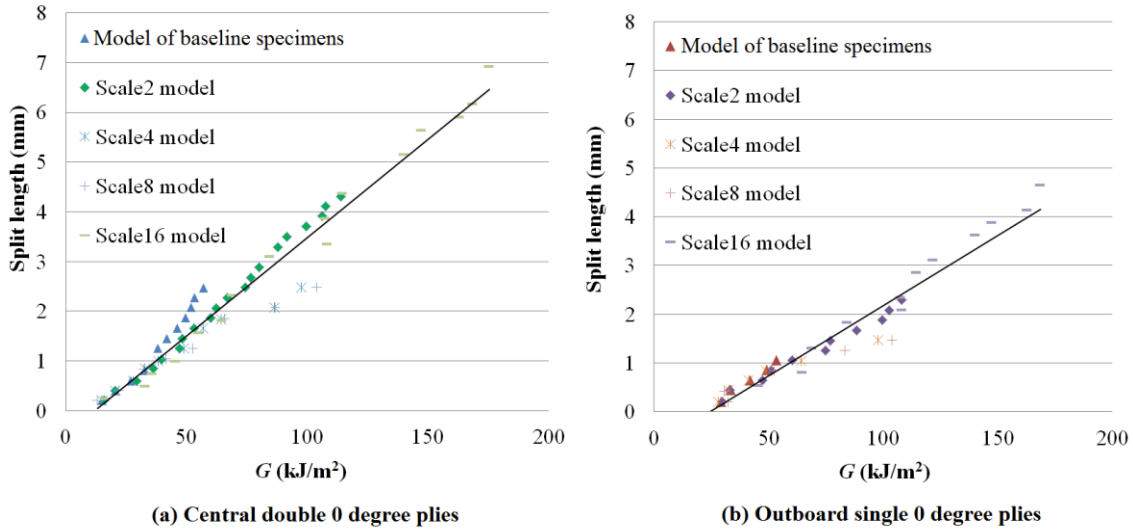

Fig. 9. Development of the initial splits in the 0° plies in scaled simpler models.

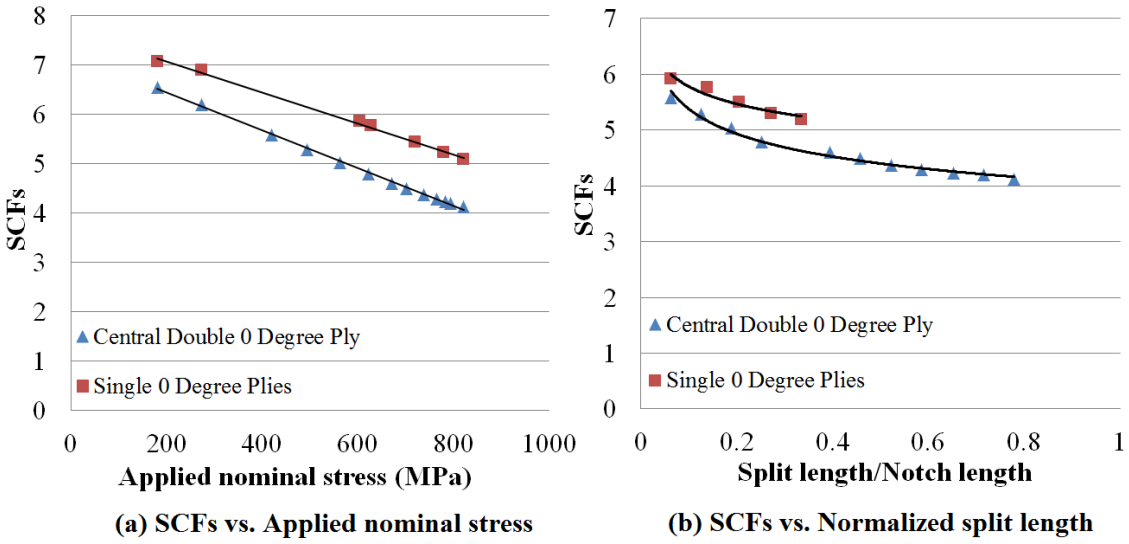

Fig. 10. Development of SCFs in the 0° plies in the simpler model of baseline specimens.

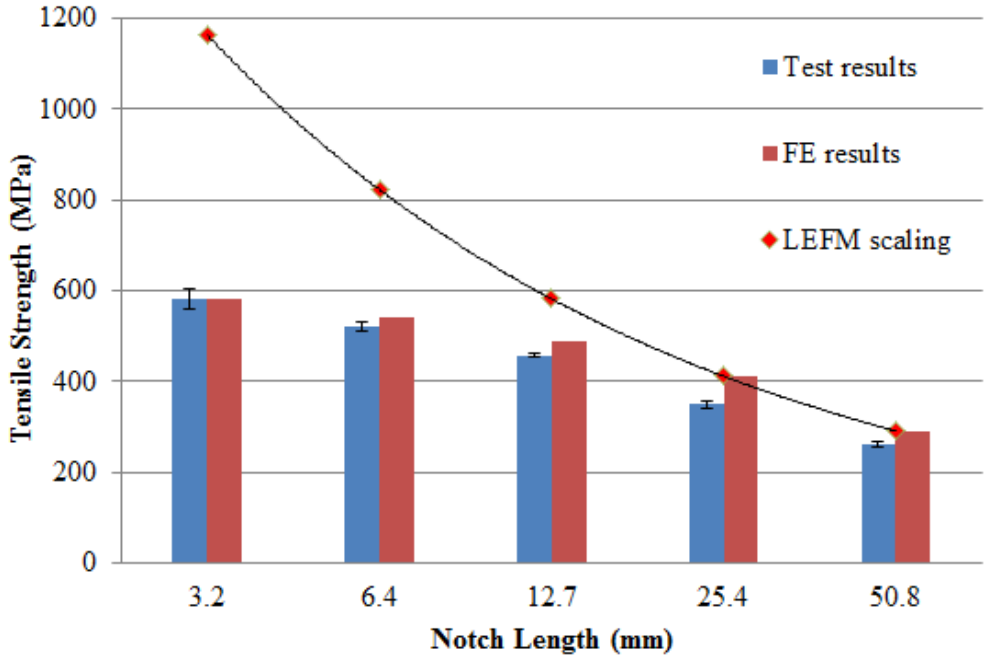

Fig. 11. Comparison of experimental and FE results.

Table 1. Properties of cohesive interface elements and lamina elements.

Properties of cohesive interface elements			
G_{IC} (N/mm)	**G_{IIC} (N/mm)**	**σ_I^{max} (MPa)**	**σ_{II}^{max} (MPa)**
0.2	1.0	60	90

Properties of lamina elements				
E_{11} (GPa)	**$E_{22}=E_{33}$ (GPa)**	**$G_{12}=G_{13}$ (GPa)**	**G_{23} (GPa)**	**Weibull modulus *m***
161	11.4	5.17	3.98	41
σ_{11}^{max} (MPa)	**$\alpha_{22}=\alpha_{33}$ ($^0C^{-1}$)**	**α_{11} ($^0C^{-1}$)**	**$\upsilon_{12}=\upsilon_{13}$**	**υ_{23}**
3131*	3×10^{-5}	0.0	0.320	0.436

* 3131 MPa is for unit volume material.